Chemical Science

ROYAL SOCIETY OF CHEMISTRY

EDGE ARTICLE

View Article Online
View Journal | View Issue

Cite this: *Chem. Sci.*, 2025, **16**, 17417

All publication charges for this article have been paid for by the Royal Society of Chemistry

Rigid cationic ligands enable high-efficiency NIR-II photoluminescence in copper(I) iodide hybrid semiconductors

Jingwen Chen,[ab] Xueqian Wu,[a] Minghui Zhang,[a] Simon J. Teat,[c] Guozhong Xu,*[b] Jingbai Li,*[a] Xiuze Hei *[a] and Jing Li *[de]

Received 22nd June 2025
Accepted 22nd August 2025

DOI: 10.1039/d5sc04588f

rsc.li/chemical-science

Near-infrared (NIR) luminescent materials are pivotal for advanced optoelectronic and biomedical applications, yet attaining efficient emission in the NIR-II region (950–1400 nm) remains challenging. Here, we introduce a ligand cationization strategy for designing copper(I) iodide-organic hybrid materials that emit in the NIR-II region (920–1120 nm) with PLQYs up to 8.58%. By incorporating rigid cationic ligands with CuI modules, we synergistically achieve bandgap narrowing (to 1.51 eV) and structural rigidification *via* ionic-dative bonding, effectively suppressing non-radiative decay while extending emission beyond 1100 nm. Coupled with solution processability—enabled by the successful synthesis of nanometer-sized nanoparticles in various shapes—and excellent thermal stability (≥210 °C), this work establishes ligand cationization as a universal approach for designing efficient NIR-II emitters.

Introduction

Near-infrared (NIR) luminescent materials (700–1400 nm) have emerged as essential components in advanced optoelectronic technologies, including bioimaging, night vision, and optical communication, due to their superior tissue penetration and minimized background interference.[1–4] While small organic molecules, perovskites, and quantum dots have successfully achieved emission in the NIR-I region (700–950 nm),[4] their extension to the longer-wavelength NIR-II range (950–1700 nm) remains challenging: organic systems are often limited by complex synthesis and low photoluminescence quantum yields (PLQYs),[5,6] whereas inorganic counterparts struggle with stability and bandgap tunability.[7,8] Copper(I) iodide-based hybrid materials (CuI-L), which integrate the structural modularity of organic ligands with the chemostability of inorganic motifs, present a compelling alternative due to their structural diversity, high stability, and unique photophysical properties.[9–11] However, existing CuI-L systems emit predominantly in the visible or short-wavelength NIR-I regions, with limited exploration of their NIR-II potential.[12–14] This limitation arises primarily from the lack of efficient strategies for bandgap narrowing and the suppression of non-radiative decay pathways.

The photoluminescence of many CuI-L hybrids arises from the excited states based on metal halide-to-ligand charge transfer process [(M + X)LCT], which is heavily influenced by ligand electronic states and structural rigidity.[10,15] Current efforts to red-shift emission wavelengths rely on extending ligand conjugation or introducing electron-withdrawing groups (EWGs) to lower the energies of the lowest unoccupied molecular orbitals (LUMOs) of ligands; however, these approaches often compromise PLQYs due to exacerbated quenching as the results of extended molecular vibrations and rotations, or fail to sufficiently narrow the bandgap.[14,16,17] This underscores the need for a unified design strategy that simultaneously tailors electronic structures and suppresses non-radiative losses effectively.

Herein, we propose a "rigid cationic ligands" strategy to engineer AIO-type[18,19] copper(I) iodide-organic hybrids (AIO-CuI-L) for tunable NIR-II photoluminescence. By incorporating a rigid, conjugated cationic center to ligands with low-lying LUMO energies, we tackle the two key challenges: bandgap narrowing and exciton stabilization (Scheme 1). This is achieved through (1) bandgap reduction *via* the enhanced electron-withdrawing effects of the cationic centers and (2) suppression of vibrational quenching as a result of rigidified inorganic–organic interfaces enabled by synergistic ionic-dative bonding.[20]

Using methylpyridinium-functionalized benzothiadiazole/benzoselenadiazole ligands, we succeed in synthesizing four different AIO-CuI-L hybrid materials with emissions in the NIR-II region (920–1120 nm) and PLQYs up to ~8.6%, surpassing

[a]*Hoffman Institute of Advanced Materials, Shenzhen Polytechnic University, Shenzhen, 518055, China. E-mail: lijingbai@szpu.edu.cn; xiuzehei@szpu.edu.cn*

[b]*College of Chemical Engineering, University of Science and Technology Liaoning, Anshan 114051, China. E-mail: gz_xu@ustl.edu.cn*

[c]*Advanced Light Source, Lawrence Berkeley National Laboratory, Berkeley, CA 94720, USA*

[d]*Department of Chemistry and Chemical Biology, Rutgers University, Piscataway, NJ 08854, USA. E-mail: jingli@rutgers.edu*

[e]*Department of Information Display, Kyung Hee University, Seoul 02447, Republic of Korea*

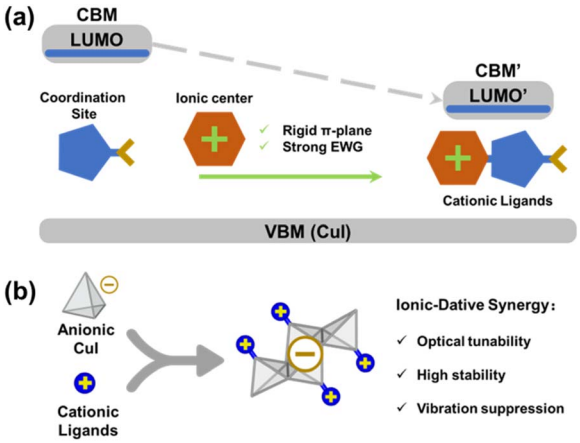

Scheme 1 Schematic illustration of "rigid cationic ligand" strategy for (a) band gap and (b) structure engineering of AIO-type CuI-L hybrid materials.

previous CuI-L systems by over 5-fold. These emitters exhibit high stability and solution processability, enabling the fabrication of uniform nanoparticles. Assisted by comprehensive optical characterizations coupled with density functional theory (DFT) analysis, this work establishes a universal design principle for functional hybrids, bridging molecular-level engineering with macroscopic optoelectronic performance.

Results and discussion

Structural description

We selected benzothiadiazole and benzoselenadiazole as core ligands as they have appropriate LUMO energy levels and strong coordination capability with CuI.[13] To further reduce the bandgap of the resulting hybrid semiconductors and enable NIR-II emission, an additional approach is necessary to further engineer these ligands. DFT calculations reveal that conventional modifications with either neutral EWGs or π-plane expansion fail to sufficiently lower the LUMO energies of benzothiadiazole and benzoselenadiazole (ΔE_{LUMO} < 0.5 eV). In sharp contrast, introducing the cationic methylpyridinium group substantially reduces their LUMO levels by ~1.5 eV (Fig. S1 and S2), leading to narrow energy gaps of the resultant CuI hybrid materials conducive to NIR-II emission. This pronounced reduction of LUMO stems primarily from the stronger electrostatic induction from the cationic center of the methylpyridinium group, which redistributes the electron density on the benzothiadiazole and benzoselenadiazole more effectively than that from the partial charges on the EWGs or the electron delocalization over the extended conjugation (Fig. S3). Furthermore, the N atoms of the cationized ligands could retain their coordination ability, forming synergistic ionic-dative bonds with CuI modules. This bonding strategy has been proven to enhance structural rigidity and stability.[12,20]

To verify the proposed strategy, we synthesized the above rigid cationic ligands by a two-step process, and their purity was confirmed with ^{1}H NMR (Fig. S4 and S5). Reactions of these ligands with CuI under different conditions yielded high-quality single crystals of the four title compounds. Single-crystal X-ray analysis revealed that their structures range from molecular 0D clusters to layered 2D networks with the formulas 0D-$Cu_2I_4(L_S)_2$ (**1**), 0D-$Cu_2I_4(L_{Se})_2$ (**2**), 1D-$Cu_6I_8(L_S)_2$ (**3**), and 2D-$Cu_6I_8(L_{Se})_2$ (**4**), as depicted in Fig. 1a–d and S8. The crystallographic data are summarized in Table S1. Notably, all compounds maintain charge neutrality through balanced coordination between cationic ligands and anionic $Cu_mI_{m+2}^{2-}$ modules, as observed in other reported AIO compounds.[18,20]

Compounds **1** and **2** share the same structure type and are isostructural, where 0D-$Cu_2I_4^{2-}$ dimeric clusters coordinate to two ligands *via* Cu–N bonds. Compound **3** consists of 1D anionic $(Cu_6I_8)^{2-}$ chains that are coordinated and charge-balanced by terminal ligands. Compound **4** is a layered structure made of 1D anionic $(Cu_6I_8)^{2-}$ chains interconnected *via* bidentate ligands. The Cu–N bond lengths in all compounds are found to be 2.03 to 2.07 Å, similar to other reported hybrid CuX-L compounds consist of Cu–N bonds.[21,22] In all compounds, Cu atoms are tetrahedrally coordinated to either three I atoms and one N atom from the ligand, or four I atoms. The coordination numbers of I atoms range from 1 to 3.

Critical to emission performance, π–π interactions between adjacent ligands were observed across all title compounds, with vertical distances (d) of 3.32–4.14 Å and displacement angles (θ) of 14.97–34.02°. Interestingly, two different kinds of π–π interactions were found in all compounds, as shown in Fig. 1e and S9. Among them, compound **3** demonstrates the most aligned π–π stacking, followed by compound **2**. The subtle geometric variations, arising from the ligand composition (S *vs.* Se) and structural dimensionality changes of CuI motifs, are anticipated to profoundly influence exciton dynamics—a hypothesis validated in subsequent photophysical studies.

High-quality single crystals and powder samples of all compounds were used for various characterizations, with their phase purity verified by powder X-ray diffraction (PXRD) analysis (Fig. S10). FT-IR spectroscopic study further validated the coordination-induced structural rigidification. As shown in Fig. 1f, taking compounds **2** and **4** as examples, the signals of the coordinated ligands remain characteristic of free ligands while showing marked attenuation of selenadiazole-related vibrations, including the N–Se–N scissoring at 720 cm^{-1}, and the β(C–H) of the phenyl-ring at 1020 and 1230 cm^{-1}. Concurrently, intensified peaks observed at 810 cm^{-1}, 1340 cm^{-1} (pyridine ring β(C–H)), and 3000–3100 cm^{-1} (methyl ν(C–H)). These spectral evolution trends, which are also consistently observed in compounds **1** and **3** (Fig. S11), arise from distinct bonding environmental changes during the Cu–N bond formation: Free ligands exhibit vibrational constraints from coulombic interactions between I^- anions and pyridinium cations, whereas coordinated ligands experience enhanced rigidity through *ionic-dative synergy*—Cu–N bonds restrict selenadiazole motions, while charge redistribution stabilizes conjugated backbones. These results demonstrate that ligand cationization not only modulates electronic structures but also imposes steric constraints to mitigate non-radiative decay pathways.

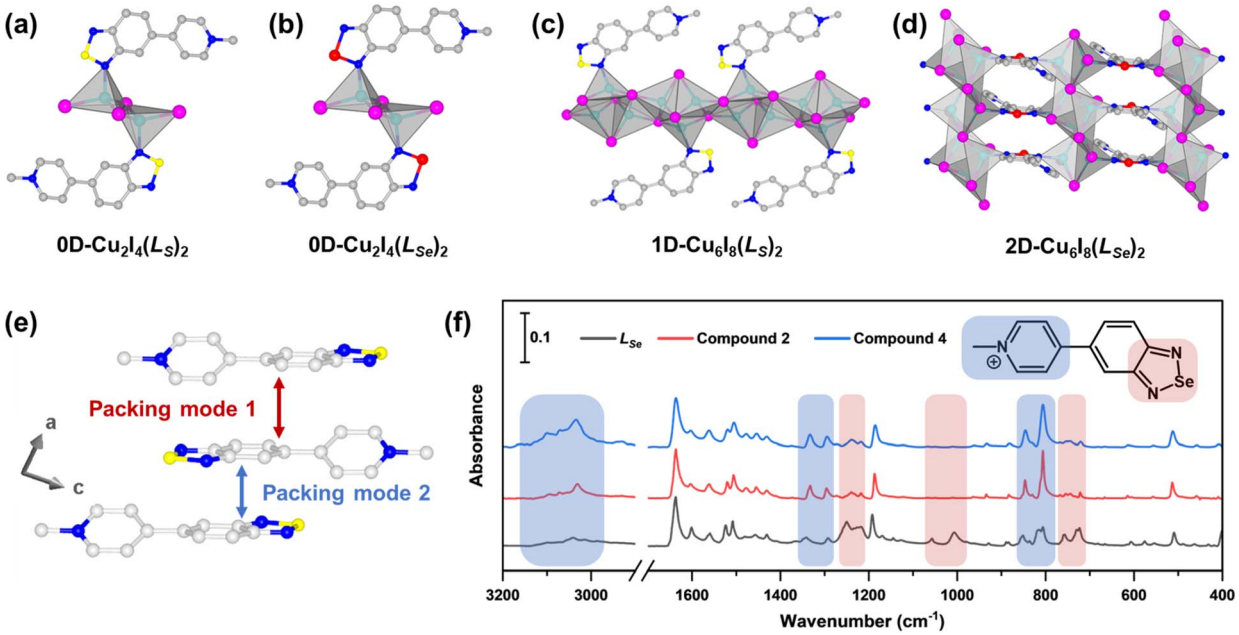

Fig. 1 Crystal structures of compounds (a) **1**, (b) **2**, (c) **3**, and (d) **4**. (e) Two different π–π packing modes within compound **1**, color scheme: cyan: Cu; purple: I; gray: C; blue: N; yellow: S; red: Se. All H atoms are omitted for clarity. (f) Experimental IR spectra of free ligand L_{Se} (black) and compounds **2** (red) and **4** (blue). The absorbance is normalized to the phenyl-ring stretching band *ν*(C=C) around 1610 cm^{-1}.

Photophysical study

The optical absorption spectra of all compounds were collected at room temperature using diffuse reflectance spectroscopy (Fig. 2a). Their optical band gaps range from 1.51 to 1.62 eV, estimated from the absorption edges using the Tauc method. The narrow band gaps are also reflected by the black colors of the samples, indicating strong visible light absorption. Room temperature photoluminescence spectroscopy reveals that upon excitation under 450 nm irradiation, all compounds

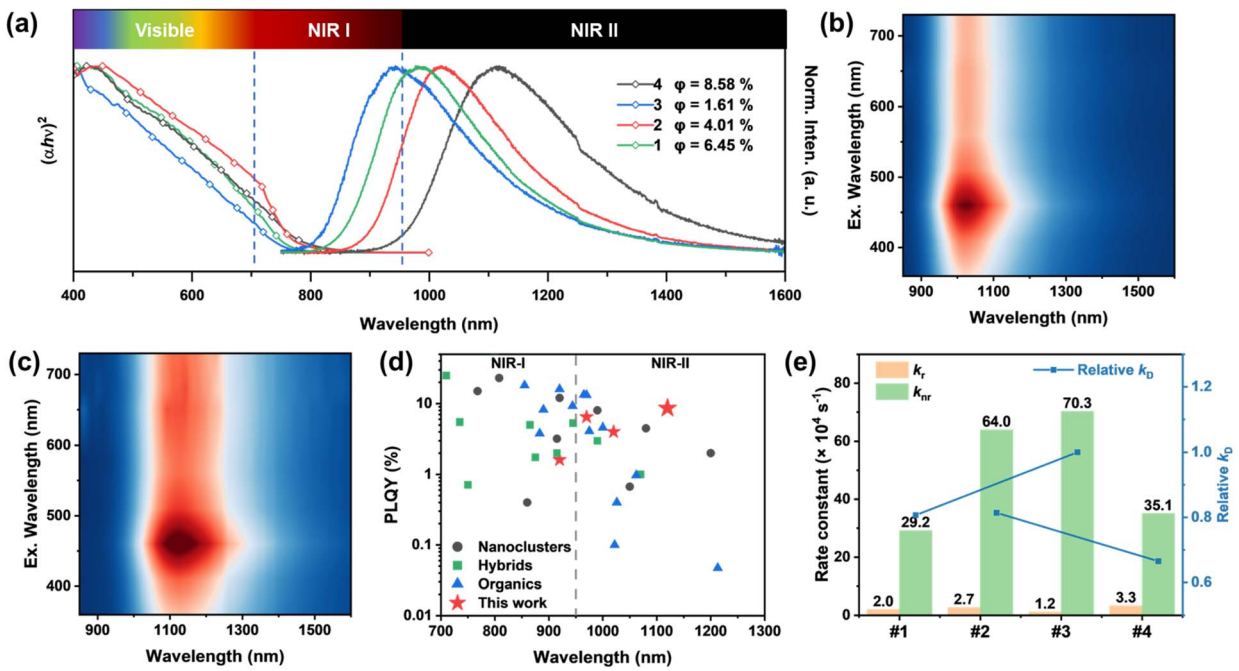

Fig. 2 (a) Optical absorption (dotted) and photoluminescence emission (solid) spectra of all compounds (λ_{ex} = 450 nm). Excitation-dependent PL spectra of compounds (b) **2** and (c) **4**. (d) PLQY for different NIR emitters in relation to their emission wavelength, detailed values and data sources can be found in Table S11. (e) The correlation between relative values of k_D with the k_r and k_{nr} values of all title compounds.

demonstrate broadband low energy emissions in the NIR-II region. The emission maxima are 970, 1020, 920 and 1120 nm for compounds **1–4**, respectively, well in trend with their estimated band gaps. Remarkably, this represents the first set of CuX-based materials that emit in the NIR-II region, surpassing the previously reported 1D-$(mqx)_2Cu_2I_4$ which exhibits the longest emission wavelength peaked at 875 nm.[13] The emission peaks and spectral shapes of all four compounds remain unchanged with varying excitation energies (Fig. 2b, c and S12), indicating a single excitation process governs their photoluminescence.[23] The full-width at half-maximum (FWHM) values of all four compounds are ~250 meV, implying the charge transfer characteristics of their excited states, similar to other reported hybrid NIR emitters.[13,24–26]

The photoluminescence quantum yields (PLQYs) of all four compounds were determined at room temperature (Fig. S13 and S14) under 450 nm excitation, as listed in Table 1. Notably, compound **4** achieved an impressive PLQY of 8.58%, with an emission peak centered at 1120 nm—setting a new record for metal-halide hybrids with simultaneously the longest emission wavelength and highest efficiency reported to date in the NIR-II region (Fig. 2d and Table S11). This dual optimization clearly outperforms conventional CuX systems (*e.g.*, PLQY of 1.7% at 875 nm),[13] underscoring the effectiveness of the "rigid cationic ligand" strategy.

To quantitatively assess their emission efficiencies, total radiative rates (k_r) and non-radiative decay rates (k_{nr}) were estimated based on eqn (1) and (2),[27,28] where η_{PL} is the PLQY value and τ_{PL} is the average PL lifetime.

$$\eta_{PL} = k_r/(k_r + k_{nr}) \quad (1)$$

$$\tau_{PL} = 1/(k_r + k_{nr}) \quad (2)$$

Note that the temperature used for PLQY and PL lifetime measurements are slightly different (RT and 278 K, respectively). Hence, the k_r are expected to be slightly underestimated and the k_{nr} are slightly overestimated. As demonstrated in Fig. 2e and Table 1, despite minor variations in k_r (1.2–3.3 × 10^4 s^{-1}), their k_{nr} differ significantly (29.2–70.3 × 10^4 s^{-1}), primarily governing PLQY differences. Such non-radiative deactivation of the photogenerated excitons can be attributed to the short-range Dexter energy-transfer process mediated by the overlap of two adjacent ligand wavefunctions, which is dominant in many NIR luminescent materials.[29–32] The energy transfer rates of Dexter coupling modes, k_D, can be estimated based on eqn (3) and are listed in Table S2, where d (vertical π–π distance), θ (displacement angle), and ω (dihedral angle) define the intermolecular coupling geometry between two π planes.[33,34]

$$k_D \propto \cos(\theta)\cdot\cos(\omega)\cdot e^{-d} \quad (3)$$

Fig. 2e correlates k_D with the k_r and k_{nr} values of all four compounds. The simultaneous increase of k_D and k_{nr} from compounds **1** to **3** (made of L_S) validates our above analysis that the enhanced π–π interactions within the structures can lead to severe non-radiative relaxations *via* Dexter energy transfer, thus reducing the PLQYs of the compounds.[35,36] For the same reason, the k_D and k_{nr} decrease from compounds **2** to **4** (made of L_{Se}). Notably, compound **1** demonstrates a k_D value comparable to **2** and higher than **4**, yet its k_{nr} remains lower than both **2** and **4**. This ligand-dependent divergence may be attributed to the van der Waals radius differences of S and Se atoms (1.80 Å and 1.90 Å, respectively),[37] as well as the significantly larger spin–orbit coupling (SOC) of Se atom, which causes apparent underestimated k_D for L_{Se} system relative to L_S system.

Temperature-dependent PL spectroscopy and lifetime measurements were carried out at various temperatures for all title compounds, as shown in Fig. 3 and S15–S17. All title compounds demonstrate little to no emission peak shifts and FWHM changes across a temperature range of 78 K to 287 K, indicative of suppressed electron-phonon coupling. Quantitative analysis through temperature-dependent FWHM evolution (eq. (4)) yielded Huang–Rhys factor (S) and photon frequency ($\hbar\omega_{photon}$),[38] while the exciton binding energies (E_b) were derived from the Arrhenius plots of the PL thermal quenching (eqn (5)),[39] as depicted in Fig. 3c and S15–S17.

$$\mathrm{FWHM} = 2.36\sqrt{S}\hbar\omega_{photon}\sqrt{\coth\frac{\hbar\omega_{photon}}{2k_BT}} \quad (4)$$

$$I(T) = \frac{I_0}{1 + A\exp\left(-\frac{E_b}{k_BT}\right)} \quad (5)$$

where k_B is the Boltzmann constant, T is the temperature, $I(T)$ is the integrated PL intensity at a specific temperature T, I_0 is the integrated PL intensity at 0 K, and A is a constant.

Owing to the unique coordination chemistry featuring strongly bonded cation–anion pairs, the title compounds demonstrate enhanced structural rigidity and strong exciton localization effects compared to many other CuX based hybrid materials,[40,41] enabled by the rigid ionic-dative frameworks. The

Table 1 Important photophysical properties of compounds **1–4**

Compound	B. G. (eV)	λ_{em} (nm)	PLQY[a] (%)	Lifetime[b] (μs)	k_r (×10^4 s^{-1})	k_{nr} (×10^4 s^{-1})	T_d[c] (°C)
1	1.60	970	6.45 ± 0.15	9.6	2.0	29.2	210
2	1.56	1020	4.01 ± 0.79	2.7	2.7	64.0	265
3	1.62	920	1.61 ± 0.46	1.7	1.2	70.3	255
4	1.51	1120	8.58 ± 0.96	2.9	3.3	35.1	275

[a] λ_{ex} = 450 nm, data obtained at RT. [b] Data obtained at 278 K. [c] T_d: decomposition temperature.

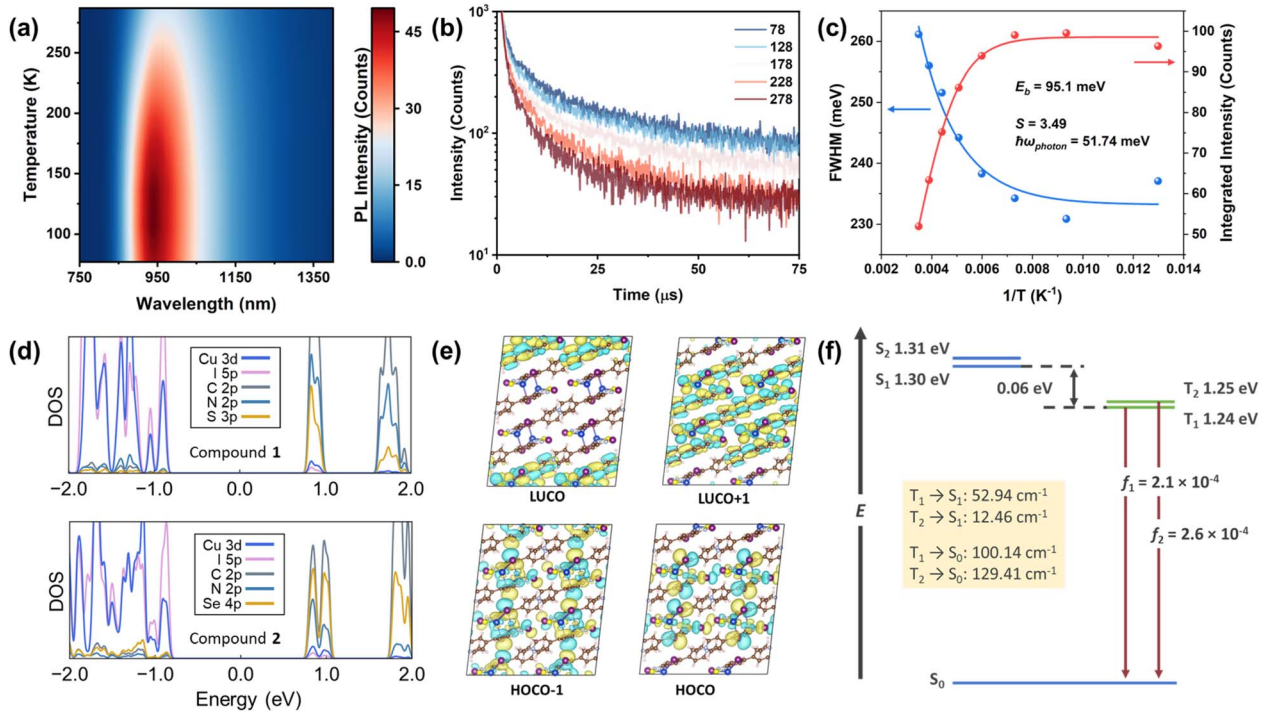

Fig. 3 (a) Temperature-dependent PL spectra, (b) PL decay curves and (c) Huang–Rhys factor (S) and exciton binding energy (E_b) fittings of compound **1**. (d) Calculated projected density of states (PDOS) of compounds **1** and **2**. (e) Calculated frontier crystal orbitals and (f) energy level diagram and SOC constant of compound **1**.

relatively smaller E_b values of compounds **2** (27.1 meV) and **3** (79.5 meV) may be attributed to their pronounced π–π interactions as described above.

All title compounds exhibit PL lifetimes at microsecond-scale across the studied temperature range (78–278 K), confirming the phosphorescence nature of their NIR emissions. Biexponential decay fittings resolved two distinct radiative pathways with amplitude ratios show little temperature-dependence (Fig. 3b, S15–S17 and Tables S3–S6). In conjunction with the observed subtle thermochromism of their emissions, these results suggest the coexistence of two weakly coupled triplet excited states (T_1 and T_2) with near-degenerate energies, which have been seen in previous studies on d^{10} metal complexes.[42,43] This phenomenon potentially arises from the different charge transfer dynamics of the differently overlapped frontier orbitals, induced by the two distinct π–π interactions observed within the structures.[44,45]

Phosphorescence mechanism

To gain insights into the role of structural features in regulating the photoluminescence mechanisms, we performed DFT calculations to study the phosphorescence mechanism of title compounds. The projected density of states (PDOS) computed with PBE0 hybrid functional show dominant contributions of Cu 3d and I 5p orbitals in the valence band maximum (VBM) and ligand orbitals (*e.g.*, p orbitals of C, N, S, Se) in the conduction band minimum (CBM), as depicted in Fig. 3d and S15. We computed the singlet and triplet excited states with time-dependent DFT (TDDFT) calculations including SOC for all title compounds, with detailed data summarized in Tables S7–S10. Fig. 3e and S16–S19 illustrate the frontier crystal orbitals participating in the electronic transitions. While the highest occupied crystal orbital (HOCO) comes from inorganic CuI modules, and the lowest unoccupied crystal orbital (LUCO) centers on the organic ligands. These results confirm that both absorption and NIR emissions of all title compounds are associated with the excited states generated from the metal halide-to-ligand charge transfer processes [(M + X)LCT], which enables facile optical tuning through ligand modifications.[19,46,47]

In compound **1**, the two distinct π–π stacking configurations in the crystal structures (Fig. 1e and S9) lead to closely spaced low-lying singlet (1.30 and 1.31 eV) and triplet (1.24 and 1.25 eV) states. The narrow energy gap between S_2 and S_1 facilitates ultrafast internal conversion to populate S_1 after photoexcitation. The S_1–T_1 and S_1–T_2 energy gaps are 0.05 and 0.06 eV, respectively. Analysis of the SOC matrix element (SOCME) reveals significantly stronger S_1–T_1 coupling (52.94 cm^{-1}) compared to S_1–T_2 (12.46 cm^{-1}), suggesting a faster intersystem crossing (ISC) from S_1 to T_1 than T_2. In contrast, the S_0–T_1 and S_0–T_2 couplings (100.10 and 129.41 cm^{-1}, respectively) are comparable, which could lead to similar non-radiative rate constants. The singlet triplet SOC introduces two low-lying spin states dominated by T_1 and T_2, responsible for two phosphorescence decay pathways. The oscillator strengths are 2.1×10^{-4} and 2.6×10^{-4} for the T_1 and T_2 featured spin states, respectively, implying comparable radiative decay rate constants from

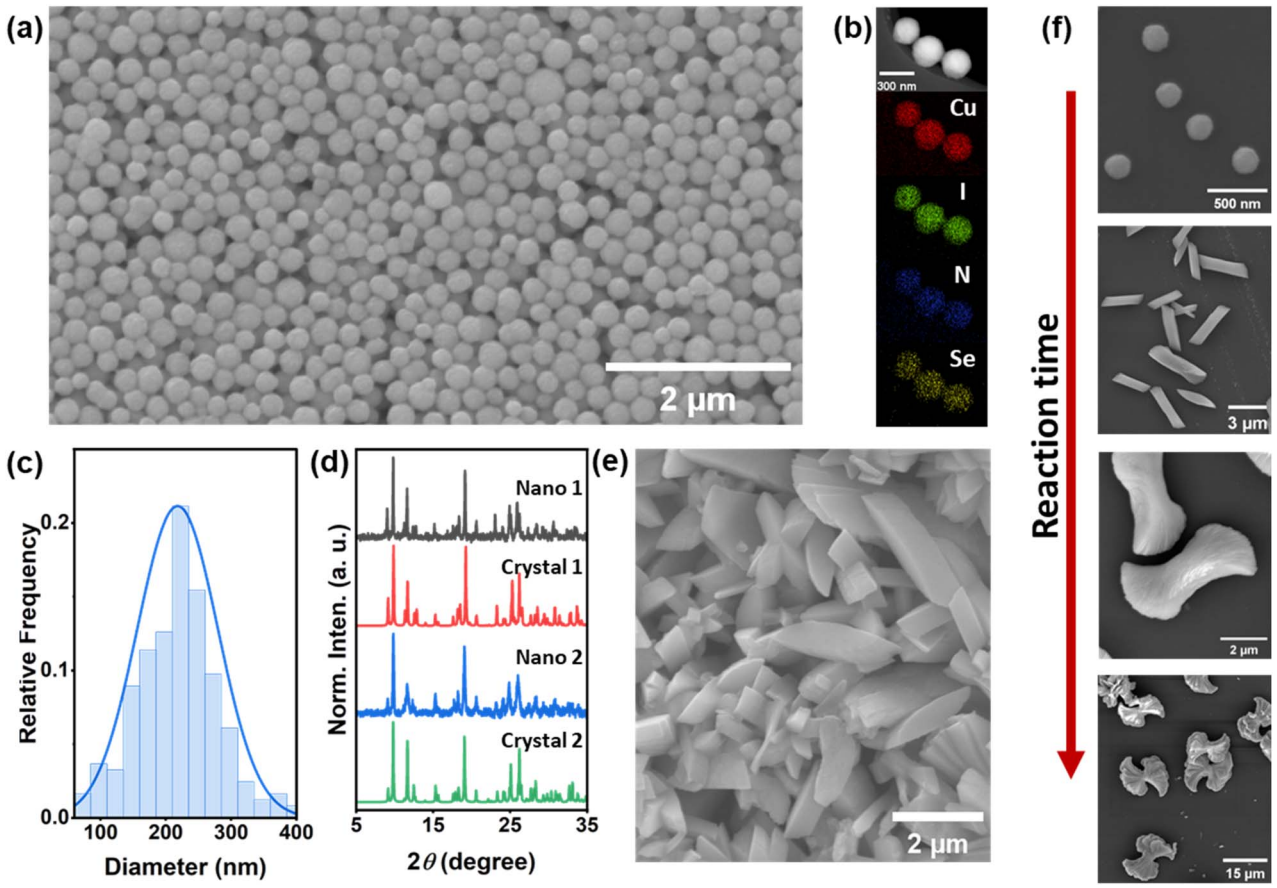

Fig. 4 (a) SEM image of the prepared nano-sized spheres of compound **2**. (b) TEM and elemental mapping images of isolated nano particles. (c) The size distribution of prepared nano particles of compound **2**. (d) PXRD patterns of two nano-sized samples of compounds **1** and **2** along with the simulated patterns. (e) SEM image of the prepared nano-rod of compound **2** with elongated reaction times. (f) The progressive morphology transformations from nanoparticles to nanoflowers as a function of time.

T_1 and T_2 to S_0. Since the phosphorescence decay is a product of both singlet-to-triplet ISC and triplet radiative transitions, the stronger SOC of T_1 with S_1 accelerates the overall phosphorescence decay relative to T_2. These computational findings, consistent across all title compounds, provide a possible explanation for the experimentally observed biexponential phosphorescence decay.

Thermal stability and processability

Thermal stability of all title compounds was assessed by thermogravimetric analysis (TGA). As shown in Fig. S20, all compounds exhibit remarkable structure robustness and remain stable up to 210 °C, with compound **4** demonstrating the highest decomposition temperature of 275 °C. In general, compounds containing Se-based ligands are more stable than those with S-based ligands, attributed to their more electron-rich coordination sites. Building extended networks to increase structural rigidity enhances stability as well, consistent with previous findings on related coordination systems.[9,48,49] Notably, the title compounds demonstrate significantly improved thermal stability compared to CuI-L hybrid structures made of charge-neutral benzothiadiazole/benzoselenadiazole ligands ($T_d \leq 150$ °C).[14] This substantial enhancement underscores the synergistic stabilization effect of ionic-dative bonding nature.

To meet the practical demands for NIR related applications, we carried out a comprehensive study to evaluate the solution processability and to develop nano-sized synthesis strategy for the title NIR emitters. The compounds demonstrate intriguing solubility in DMSO, despite their structural rigidity, evidenced by the ^{1}H NMR spectra of dissolved compounds (Fig. S6 and S7). Consistent with previous studies, the dissolved species were identified as small fragments of anionic CuI clusters remaining coordinated to cationic ligands,[28,50] and the reversibility of this dissolution process was confirmed by recrystallizations. Besides this solution processability, we further synthesized nano-sized samples with high dispersibility. Taking compound **2** as an example: Uniformly shaped nanoparticles were formed upon rapid injection of ligand solutions into a CuI/KI/PVP colloidal mixture at 70 °C. Scanning electron microscopy (SEM) revealed spherical nanoparticles (~210 nm in diameter, Fig. 4) with smooth surfaces, while TEM-EDS elemental mapping further confirmed the homogeneous spatial distribution of constituent elements (Cu, I, N, Se) within individual nanoparticles. The phase purity was validated by well-matched experimental and

simulated PXRD patterns, retained FT-IR vibrational signatures, and consistent UV-Vis absorption edges, as shown in Fig. 4 and S21. Interestingly, progressive structural transformations from initial nanospheres (~210 nm) to elongated nanorods (~3 μm), followed by centrally constricted intermediates (~5 μm), and ultimately hierarchical nanoflowers (15–20 μm) were observed through timed reaction processes (Reaction time: 1 s, 5 s, 15 s and 1 min, respectively). Similar size/morphology progression was also observed for compound **1** (Fig. S22), enabling customizable light–matter interactions for targeted applications, *via* nanostructure tuning.

Conclusions

In this work, we have designed and synthesized a series of four narrow bandgap CuI-based hybrid semiconductor materials made of anionic $Cu_nI_{n+2}^{2-}$ and cationic ligands. All compounds emit in NIR-II region (920–1120 nm) with PLQY up to 8.58%. The cationic centers induce a strong electron-withdrawing effect to the coordination core, thus lowering the LUMO energy of the ligands and reducing the bandgap effectively, while the rigid ionic-dative bonding network suppresses non-radiative decay by restricting molecular vibrations. This dual functionality renders those materials efficient photoluminescence in NIR-II region. Coupled with processability for nano structural control (210 nm nanoparticles to 20 μm nanoflowers), and thermal resilience (≥210 °C), this cationization-driven bandgap engineering provides a new possibility for high-performance NIR-II materials.

Author contributions

J. W. Chen: formal analysis, investigation, writing – original draft; X. Q. Wu: investigation, formal analysis; M. H. Zhan: investigation, formal analysis; S. J. Teat: investigation, formal analysis, resources; G. Z. Xu: validation, supervision; J. B. Li: formal analysis, validation, writing – review & editing; X. Z. Hei: conceptualization, funding acquisition, writing – review & editing, supervision, project administration; J. Li: conceptualization, writing – review & editing, supervision, project administration.

Conflicts of interest

There are no conflicts to declare.

Data availability

Supplementary Information: Methods, ^{1}H NMR spectroscopy, Crystal data and structural plots, photophysical properties, DFT calculations, thermal stability and processibility. The data supporting this article can be found in the SI. See DOI: **https://doi.org/10.1039/d5sc04588f**.

Acknowledgements

The authors acknowledge the financial support from Shenzhen Science and Technology Program (grant no. 20231124150717002 and No. RCBS20231211090634054), Guangdong Basic and Applied Basic Research Foundation (grant no. 2023A1515110006) and National Science Foundation of China grants (22303053). This research used the Advanced Light Source (ALS), which is a DOE Office of Science User Facility under contract no. DE-AC02-05CH11231.

References

1 Y. Gu, Z. Guo, W. Yuan, M. Kong, Y. Liu, Y. Liu, Y. Gao, W. Feng, F. Wang, J. Zhou, D. Jin and F. Li, High-sensitivity imaging of time-domain near-infrared light transducer, *Nat. Photonics*, 2019, **13**, 525–531.

2 Y.-C. Wei, S. F. Wang, Y. Hu, L.-S. Liao, D.-G. Chen, K.-H. Chang, C.-W. Wang, S.-H. Liu, W.-H. Chan, J.-L. Liao, W.-Y. Hung, T.-H. Wang, P.-T. Chen, H.-F. Hsu, Y. Chi and P.-T. Chou, Overcoming the energy gap law in near-infrared OLEDs by exciton–vibration decoupling, *Nat. Photonics*, 2020, **14**, 570–577.

3 A. Minotto, I. Bulut, A. G. Rapidis, G. Carnicella, M. Patrini, E. Lunedei, H. L. Anderson and F. Cacialli, Towards efficient near-infrared fluorescent organic light-emitting diodes, *Light: Sci. Appl.*, 2021, **10**, 18.

4 M. Vasilopoulou, A. Fakharuddin, F. P. García de Arquer, D. G. Georgiadou, H. Kim, A. R. b. Mohd Yusoff, F. Gao, M. K. Nazeeruddin, H. J. Bolink and E. H. Sargent, Advances in solution-processed near-infrared light-emitting diodes, *Nat. Photonics*, 2021, **15**, 656–669.

5 H. Guo, Q. Peng, X.-K. Chen, Q. Gu, S. Dong, E. W. Evans, A. J. Gillett, X. Ai, M. Zhang, D. Credgington, V. Coropceanu, R. H. Friend, J.-L. Brédas and F. Li, High stability and luminescence efficiency in donor–acceptor neutral radicals not following the Aufbau principle, *Nat. Mater.*, 2019, **18**, 977–984.

6 Q. Zhang, R. Wang, B. Feng, X. Zhong and K. Ostrikov, Photoluminescence mechanism of carbon dots: triggering high-color-purity red fluorescence emission through edge amino protonation, *Nat. Commun.*, 2021, **12**, 6856.

7 Y.-H. Jia, S. Neutzner, Y. Zhou, M. Yang, J. M. F. Tapia, N. Li, H. Yu, J. Cao, J.-P. Wang, A. Petrozza, C.-P. Wong and N. Zhao, Role of Excess FAI in Formation of High-Efficiency $FAPbI_3$-Based Light-Emitting Diodes, *Adv. Funct. Mater.*, 2020, **30**, 1906875.

8 Y. Liu, F. Di Stasio, C. Bi, J. Zhang, Z. Xia, Z. Shi and L. Manna, Near-Infrared Light Emitting Metal Halides: Materials, Mechanisms, and Applications, *Adv. Mater.*, 2024, **36**, 2312482.

9 X. Hei and J. Li, All-in-one: a new approach toward robust and solution-processable copper halide hybrid semiconductors by integrating covalent, coordinate and ionic bonds in their structures, *Chem. Sci.*, 2021, **12**, 3805–3817.

10 J. Troyano, F. Zamora and S. Delgado, Copper(i)–iodide cluster structures as functional and processable platform materials, *Chem. Soc. Rev.*, 2021, **50**, 4606–4628.
11 V. W.-W. Yam, V. K.-M. Au and S. Y.-L. Leung, Light-Emitting Self-Assembled Materials Based on d8 and d10 Transition Metal Complexes, *Chem. Rev.*, 2015, **115**, 7589–7728.
12 W. Liu, Y. Fang and J. Li, Copper Iodide Based Hybrid Phosphors for Energy-Efficient General Lighting Technologies, *Adv. Funct. Mater.*, 2018, **28**, 1705593.
13 K. Zhu, G. M. Carignan, S. J. Teat, S. Rangan, X. Hei, L. H. Nguyen and J. Li, Narrow Band Gap Hybrid Copper(I) Iodides: Designer Materials for Optoelectronic Applications, *Chem. Mater.*, 2024, **36**, 11139–11149.
14 Y. Fang, K. Zhu, S. J. Teat, O. G. Reid, X. Hei, K. Zhu, X. Fang, M. Li, C. A. Sojdak, M. Cotlet and J. Li, Robust and Highly Conductive Water-Stable Copper Iodide-Based Hybrid Single Crystals, *Chem. Mater.*, 2022, **34**, 10040–10049.
15 D. A. Popy and B. Saparov, "This or that" – light emission from hybrid organic–inorganic vs. coordination Cu(i) halides, *J. Mater. Chem. C*, 2025, **13**, 521–560.
16 H. Miao, Y. Zhou, P. Wang, Z. Huang, W. Zhaxi, L. Liu, F. Duan, J. Wang, X. Ma, S. Jiang, W. Huang, Q. Zhang and D. Wu, High-temperature negative thermal quenching phosphors from molecular-based materials, *Chem. Commun.*, 2023, **59**, 1229–1232.
17 R. Kobayashi, H. Kihara, T. Kusukawa, H. Imoto and K. Naka, Dinuclear Rhombic Copper(I) Iodide Complexes with Rigid Bidentate Arsenic Ligands, *Chem. Lett.*, 2021, **50**, 382–385.
18 W. Liu, K. Zhu, S. J. Teat, G. Dey, Z. Shen, L. Wang, D. M. O'Carroll and J. Li, All-in-One: Achieving Robust, Strongly Luminescent and Highly Dispersible Hybrid Materials by Combining Ionic and Coordinate Bonds in Molecular Crystals, *J. Am. Chem. Soc.*, 2017, **139**, 9281–9290.
19 X. Hei, W. Liu, K. Zhu, S. J. Teat, S. Jensen, M. Li, D. M. O'Carroll, K. Wei, K. Tan, M. Cotlet, T. Thonhauser and J. Li, Blending Ionic and Coordinate Bonds in Hybrid Semiconductor Materials: A General Approach toward Robust and Solution-Processable Covalent/Coordinate Network Structures, *J. Am. Chem. Soc.*, 2020, **142**, 4242–4253.
20 X. Hei and J. Li, Making coordination networks ionic: a unique strategy to achieve solution-processable hybrid semiconductors, *Mater. Chem. Front.*, 2023, **7**, 4598–4604.
21 W. Ki, X. Hei, H. T. Yi, W. Liu, S. J. Teat, M. Li, Y. Fang, V. Podzorov, E. Garfunkel and J. Li, Two-Dimensional Copper Iodide-Based Inorganic–Organic Hybrid Semiconductors: Synthesis, Structures, and Optical and Transport Properties, *Chem. Mater.*, 2021, **33**, 5317–5325.
22 X. Hei, K. Zhu, G. Carignan, S. J. Teat, M. Li, G. Zhang, M. Bonite and J. Li, Solution-processable copper(I) iodide-based inorganic-organic hybrid semiconductors composed of both coordinate and ionic bonds, *J. Solid State Chem.*, 2022, **314**, 123427.
23 M. Xie, C. Han, Q. Liang, J. Zhang, G. Xie and H. Xu, Highly efficient sky blue electroluminescence from ligand-activated copper iodide clusters: Overcoming the limitations of cluster light-emitting diodes, *Sci. Adv.*, 2019, **5**, eaav9857.
24 B. Su, S. Geng, Z. Xiao and Z. Xia, Highly Distorted Antimony(III) Chloride $[Sb_2Cl_8]^{2-}$ Dimers for Near-Infrared Luminescence up to 1070 nm, *Angew. Chem., Int. Ed.*, 2022, **61**, e202208881.
25 V. Morad, Y. Shynkarenko, S. Yakunin, A. Brumberg, R. D. Schaller and M. V. Kovalenko, Disphenoidal Zero-Dimensional Lead, Tin, and Germanium Halides: Highly Emissive Singlet and Triplet Self-Trapped Excitons and X-ray Scintillation, *J. Am. Chem. Soc.*, 2019, **141**, 9764–9768.
26 B. Li, J. Jin, M. Yin, X. Zhang, M. S. Molokeev, Z. Xia and Y. Xu, Sequential and Reversible Phase Transformations in Zero-Dimensional Organic-Inorganic Hybrid Sb-based Halides towards Multiple Emissions, *Angew. Chem., Int. Ed.*, 2022, **61**, e202212741.
27 T. M. Kirse, I. Maisuls, L. Spierling, A. Hepp, J. Kösters and C. A. Strassert, One Dianionic Luminophore with Three Coordination Modes Binding Four Different Metals: Toward Unexpectedly Phosphorescent Transition Metal Complexes, *Adv. Sci.*, 2024, **11**, 2306801.
28 J. Chen, K. Zhou, J. Li, G. Xu, X. Hei and J. Li, Strongly photoluminescent and radioluminescent copper(i) iodide hybrid materials made of coordinated ionic chains, *Chem. Sci.*, 2025, **16**, 1106–1114.
29 F. Witte, P. Rietsch, N. Nirmalananthan-Budau, F. Weigert, J. P. Götze, U. Resch-Genger, S. Eigler and B. Paulus, Aggregation-induced emission leading to two distinct emissive species in the solid-state structure of high-dipole organic chromophores, *Phys. Chem. Chem. Phys.*, 2021, **23**, 17521–17529.
30 M. Zhao, M. Li, W. Li, S. Du, Z. Chen, M. Luo, Y. Qiu, X. Lu, S. Yang, Z. Wang, J. Zhang, S.-J. Su and Z. Ge, Highly Efficient Near-Infrared Thermally Activated Delayed Fluorescent Emitters in Non-Doped Electroluminescent Devices, *Angew. Chem., Int. Ed.*, 2022, **61**, e202210687.
31 C. Ou, L. An, Z. Zhao, F. Gao, L. Zheng, C. Xu, K. Zhang, J. Shao, L. Xie and X. Dong, Promoting near-infrared II fluorescence efficiency by blocking long-range energy migration, *Aggregate*, 2023, **4**, e290.
32 X.-Y. Dai, M. Huo and Y. Liu, Phosphorescence resonance energy transfer from purely organic supramolecular assembly, *Nat. Rev. Chem.*, 2023, **7**, 854–874.
33 P. Srujana, P. Sudhakar and T. P. Radhakrishnan, Enhancement of fluorescence efficiency from molecules to materials and the critical role of molecular assembly, *J. Mater. Chem. C*, 2018, **6**, 9314–9329.
34 P. Srujana and T. P. Radhakrishnan, Establishing the Critical Role of Oriented Aggregation in Molecular Solid State Fluorescence Enhancement, *Chem.–Eur. J.*, 2018, **24**, 1784–1788.
35 A. Cravcenco, C. Ye, J. Gräfenstein and K. Börjesson, Interplay between Förster and Dexter Energy Transfer Rates in Isomeric Donor–Bridge–Acceptor Systems, *J. Phys. Chem. A*, 2020, **124**, 7219–7227.
36 G. Li, D. Jiang, G. Shan, W. Song, J. Tong, D. Kang, B. Hou, Y. Mu, K. Shao, Y. Geng, X. Wang and Z. Su, Organic Supramolecular Zippers with Ultralong Organic

Phosphorescence by a Dexter Energy Transfer Mechanism, *Angew. Chem., Int. Ed.*, 2022, **61**, e202113425.

37 A. Bondi, van der Waals Volumes and Radii, *J. Phys. Chem.*, 1964, **68**, 441–451.

38 W. Stadler, D. M. Hofmann, H. C. Alt, T. Muschik, B. K. Meyer, E. Weigel, G. Müller-Vogt, M. Salk, E. Rupp and K. W. Benz, Optical investigations of defects in Cd1-xZnxTe, *Phys. Rev. B*, 1995, **51**, 10619–10630.

39 J.-H. Wei, J.-F. Liao, L. Zhou, J.-B. Luo, X.-D. Wang and D.-B. Kuang, Indium-antimony-halide single crystals for high-efficiency white-light emission and anti-counterfeiting, *Sci. Adv.*, 2021, **7**, eabg3989.

40 T. Xu, Y. Li, M. Nikl, R. Kucerkova, Z. Zhou, J. Chen, Y.-Y. Sun, G. Niu, J. Tang, Q. Wang, G. Ren and Y. Wu, Lead-Free Zero-Dimensional Organic-Copper(I) Halides as Stable and Sensitive X-ray Scintillators, *ACS Appl. Mater. Interfaces*, 2022, **14**, 14157–14164.

41 S. Fang, B. Zhou, H. Li, H. Hu, H. Zhong, H. Li and Y. Shi, Highly Reversible Moisture-Induced Bright Self-Trapped Exciton Emissions in a Copper-Based Organic–Inorganic Hybrid Metal Halide, *Adv. Opt. Mater.*, 2022, **10**, 2200605.

42 R. Hamze, J. L. Peltier, D. Sylvinson, M. Jung, J. Cardenas, R. Haiges, M. Soleilhavoup, R. Jazzar, P. I. Djurovich, G. Bertrand and M. E. Thompson, Eliminating nonradiative decay in Cu(I) emitters: >99% quantum efficiency and microsecond lifetime, *Science*, 2019, **363**, 601–606.

43 X. Hei, S. J. Teat, M. Li, M. Bonite and J. Li, Highly soluble copper(i) iodide-based hybrid luminescent semiconductors containing molecular and one-dimensional coordinated anionic inorganic motifs, *J. Mater. Chem. C*, 2023, **11**, 3086–3094.

44 M.-Y. Leung, M.-C. Tang, W.-L. Cheung, S.-L. Lai, M. Ng, M.-Y. Chan and V. Wing-Wah Yam, Thermally Stimulated Delayed Phosphorescence (TSDP)-Based Gold(III) Complexes of Tridentate Pyrazine-Containing Pincer Ligand with Wide Emission Color Tunability and Their Application in Organic Light-Emitting Devices, *J. Am. Chem. Soc.*, 2020, **142**, 2448–2459.

45 H. Wang, H. Ma, N. Gan, K. Qin, Z. Song, A. Lv, K. Wang, W. Ye, X. Yao, C. Zhou, X. Wang, Z. Zhou, S. Yang, L. Yang, C. Bo, H. Shi, F. Huo, G. Li, W. Huang and Z. An, Abnormal thermally-stimulated dynamic organic phosphorescence, *Nat. Commun.*, 2024, **15**, 2134.

46 X. Hei, S. J. Teat, M. Li, M. Bonite and J. Li, Solution-Processable Copper Halide Based Hybrid Materials Consisting of Cationic Ligands with Different Coordination Modes, *Inorg. Chem.*, 2023, **62**, 3660–3668.

47 X. Hei, S. J. Teat, W. Liu and J. Li, Eco-friendly, solution-processable and efficient low-energy lighting phosphors: copper halide based hybrid semiconductors $Cu_4X_6(L)_2$ (X = Br, I) composed of covalent, ionic and coordinate bonds, *J. Mater. Chem. C*, 2020, **8**, 16790–16797.

48 Y. Fang, W. Liu, S. J. Teat, G. Dey, Z. Shen, L. An, D. Yu, L. Wang, D. M. O'Carroll and J. Li, A Systematic Approach to Achieving High Performance Hybrid Lighting Phosphors with Excellent Thermal- and Photostability, *Adv. Funct. Mater.*, 2017, **27**, 1603444.

49 W. Liu, Y. Fang, G. Z. Wei, S. J. Teat, K. Xiong, Z. Hu, W. P. Lustig and J. Li, A Family of Highly Efficient CuI-Based Lighting Phosphors Prepared by a Systematic, Bottom-up Synthetic Approach, *J. Am. Chem. Soc.*, 2015, **137**, 9400–9408.

50 A. V. Artem'ev, E. A. Pritchina, M. I. Rakhmanova, N. P. Gritsan, I. Y. Bagryanskaya, S. F. Malysheva and N. A. Belogorlova, Alkyl-dependent self-assembly of the first red-emitting zwitterionic $\{Cu_4I_6\}$ clusters from $[alkyl\text{-}P(2\text{-}Py)_3]^+$ salts and CuI: when size matters, *Dalton Trans.*, 2019, **48**, 2328–2337.